



## OPEN ACCESS

# Unravelling the complex drug–drug interactions of the cardiovascular drugs, verapamil and digoxin, with P-glycoprotein

Kaitlyn V. Ledwitch\*, Robert W. Barnes\* and Arthur G. Roberts\*<sup>1</sup>

\*Department of Pharmaceutical and Biomedical Sciences, University of Georgia, Athens, GA 30602, U.S.A.

## Synopsis

Drug–drug interactions (DDIs) and associated toxicity from cardiovascular drugs represents a major problem for effective co-administration of cardiovascular therapeutics. A significant amount of drug toxicity from DDIs occurs because of drug interactions and multiple cardiovascular drug binding to the efflux transporter P-glycoprotein (Pgp), which is particularly problematic for cardiovascular drugs because of their relatively low therapeutic indexes. The calcium channel antagonist, verapamil and the cardiac glycoside, digoxin, exhibit DDIs with Pgp through non-competitive inhibition of digoxin transport, which leads to elevated digoxin plasma concentrations and digoxin toxicity. In the present study, verapamil-induced ATPase activation kinetics were biphasic implying at least two verapamil-binding sites on Pgp, whereas monophasic digoxin activation of Pgp-coupled ATPase kinetics suggested a single digoxin-binding site. Using intrinsic protein fluorescence and the saturation transfer double difference (STDD) NMR techniques to probe drug–Pgp interactions, verapamil was found to have little effect on digoxin–Pgp interactions at low concentrations of verapamil, which is consistent with simultaneous binding of the drugs and non-competitive inhibition. Higher concentrations of verapamil caused significant disruption of digoxin–Pgp interactions that suggested overlapping and competing drug-binding sites. These interactions correlated to drug-induced conformational changes deduced from acrylamide quenching of Pgp tryptophan fluorescence. Also, Pgp-coupled ATPase activity kinetics measured with a range of verapamil and digoxin concentrations fit well to a DDI model encompassing non-competitive and competitive inhibition of digoxin by verapamil. The results and previous transport studies were combined into a comprehensive model of verapamil–digoxin DDIs encompassing drug binding, ATP hydrolysis, transport and conformational changes.

**Key words:** ABC transporter, cardiovascular, drug transport, fluorescence, NMR.

Cite this article as: Bioscience Reports (2016) 36, e00309, doi:10.1042/BSR20150317

## INTRODUCTION

Drug–drug interactions (DDIs) involving cardiovascular therapeutics and their related toxicity continue to represent serious challenges to effective treatment of patients with heart disease [1–5]. In one previous [5] study, DDIs from co-administration of cardiovascular drugs were implicated in ~50% of adverse drug reactions in patients receiving therapy. The P-glycoprotein (Pgp) transporter is an ATP-powered efflux pump that plays a major role in cardiovascular DDIs and effluxes a diverse range of cardiovascular therapeutics [6,7]. The transporter is expressed in the brain, intestines, liver, placenta and the kidneys [8,9] and

at relatively low levels in the heart [10]. The expression level is also influenced by genetic polymorphisms and cardiomyopathy [11,12].

DDIs with the transporter occur because many cardiovascular drugs are substrates for and functional inhibitors of the transporter [4,7,13,14]. This is particularly problematic for cardiovascular drugs with relatively low therapeutic indexes such as antiarrhythmic drugs and oral anticoagulants because co-administration with these drugs can lead to elevated drug plasma concentrations and increased toxicity [7].

The calcium channel blocker verapamil (Figure 1A), which is commonly used to control hypertension, chest pain and arrhythmia [15–19], functions as a substrate and an inhibitor of the

**Abbreviations:** COPASI, complex pathway simulator; DDI, drug–drug interaction; DDM, *n*-dodecyl- $\beta$ -D-maltoside; EGTA, ethylene glycol tetraacetic acid; L, ligand; NATA, *N*-acetyl-L-tryptophanamide; NBD, nucleotide-binding domain; Ni-NTA, nickel-nitrilotriacetic acid; Pgp, P-glycoprotein; STD, saturation transfer difference; STDD, saturation transfer double difference.

<sup>1</sup> To whom the correspondence should be addressed (email audie@uga.edu).

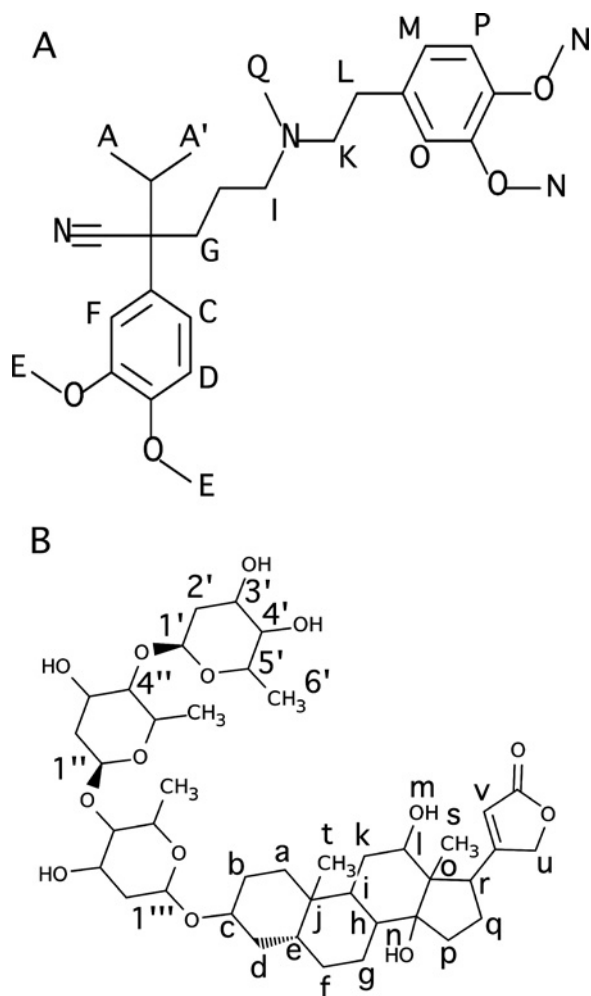


**Figure 1** Molecular structures of (A) verapamil and (B) digoxin with the nuclei labelled

transporter [7]. From results of *in vitro* studies, the drug is known to activate Pgp-coupled ATP-hydrolysis [20]. This drug manifests a spectrum of characteristics, ranging from being a good substrate to a non-substrate for the transporter, which depends on the cell type being evaluated in *in vitro* cell studies [21–26] or host tissue type in *in vivo* studies [27–29]. Although the actual molecular details of these interactions are currently unknown, the drug has been shown to inhibit the ATPase activity of a second drug by competitive, non-competitive and allosteric mechanisms in an *in vitro* study [30]. Verapamil has also been shown to inhibit cardiovascular drug transport by human Pgp *in vivo* [4,31,32].

The cardiac glycoside digoxin (Figure 1B), which has a relatively low therapeutic index, is widely used to treat atrial fibrillation and heart failure [33]. The drug is primarily excreted by the Pgp transporter in the kidneys [34,35]. Importantly, this drug is often co-administered with verapamil, which is known to non-competitively inhibit human Pgp-mediated digoxin trans-

port based upon *in vitro* studies [36,37]. These findings strongly suggest that both drugs are simultaneously bound to the transporter. Inhibition of human Pgp transport by verapamil *in vivo* is known to decrease the extent of renal tubular elimination of digoxin. This finding correlated with increased digoxin blood plasma concentrations from 60 to 90% [32,36] and lead to adverse drug reactions from digoxin toxicity [31,38].

Because verapamil and digoxin have been the focus of a number of *in vitro* [20] and *in vivo* studies [27], these drugs are ideal for studying DDIs with the transporter. Many molecular and mechanistic details of verapamil–digoxin DDIs with Pgp remain unresolved. This information is essential for defining a general DDI mechanism, for identifying therapeutics that have a high probability of exhibiting DDIs with Pgp and for ameliorating DDIs from commercially available therapeutics with Pgp.

The effect of verapamil and digoxin on the Pgp-coupled ATPase activity, the interactions of verapamil and digoxin with Pgp and the effect of verapamil and digoxin on Pgp conformation were investigated with Pgp reconstituted into liposomes. The drug-induced ATPase activation kinetics of Pgp in the presence of verapamil and digoxin allowed us to estimate the minimum number of drug-binding sites. To explore the effect of verapamil on the affinity of digoxin, digoxin's affinity to Pgp in the presence of several verapamil concentrations was estimated using intrinsic protein fluorescence. The molecular interactions between the drugs and Pgp were investigated by the saturation transfer double difference (STDD) NMR technique. Drug-induced effects on Pgp conformation were studied by acrylamide quenching of tryptophan fluorescence. Additionally, Pgp-coupled ATPase activity kinetics were measured with a panel of verapamil and digoxin concentrations, and fit to a DDI model of drug-induced ATPase activation. This information was combined with previous transport studies to produce a comprehensive mechanistic and molecular model of verapamil–digoxin DDIs.

## EXPERIMENTAL

### Materials

Verapamil hydrochloride was purchased from Fagron. Digoxin, ethylene glycol tetraacetic acid (EGTA) and imidazole were purchased from Alfa Aesar. The detergent used in protein purification, *n*-dodecyl- $\beta$ -D-maltoside (DDM), was purchased from EMD Millipore Corporation. *Escherichia coli* total lipid extract powder was purchased from Avanti Polar Lipids Inc. DTT was purchased from Gold Biotechnology. Deuterium oxide ( $^2\text{H}_2\text{O}$ ) was purchased from Cambridge Isotope Laboratories. The remaining chemicals were purchased from Sigma–Aldrich.

### Expression and purification of the mouse Pgp transporter

The wild-type His-tagged mouse Pgp transporter was purified from *Pichia pastoris* as described with some modifications

[39,40]. The yeast cells were grown and induced with methanol at the Bioexpression and Fermentation Facility at the University of Georgia in a 32 l DCI-Biolafitte fermenter with a 20 l working volume using a similar strategy as [40]. Instead of using glass bead breaking or the French press to crack the yeast cells [39,40], the cells were cracked by a minimum of six passes by liquid nitrogen freezing and blending [41]. To reduce the amount of DDM in our activity assays and during liposome preparation, no additional DDM was added after the nickel-nitrilotriacetic acid (Ni-NTA) column step. Typical protein purification yields were  $12 \pm 2$  mg for 100 g of wet weight cells, which is similar to previous yields [39]. SDS/PAGE analysis of the protein showed that it was >95 % pure. The protein was concentrated up to  $150 \mu\text{M}$  in Amicon Ultra-15 100 kDa cut-off filters (EMD Millipore, Billerica, MA) and stored at  $-80^\circ\text{C}$  in 10 mM Tris/HCl, 30 % glycerol, pH 8.0. The concentration of detergent-solubilized Pgp was measured using the DC Protein Assay Kit II (Bio-Rad Laboratories) or using the molar absorption coefficient of  $1.28 \text{ ml}\cdot\text{mg}^{-1}\cdot\text{cm}^{-1}$  ( $0.181 \mu\text{M}^{-1}\cdot\text{cm}^{-1}$ ) [39].

### Reconstitution of Pgp into liposomes

Pgp was reconstituted into 400 nm unilamellar liposomes using the filter extrusion method [42,43]. The liposomes were composed of 80 % w/v Avanti *E. coli* Total Lipid Extract (Avanti Polar Lipids) with a defined lipid profile and 20 % w/v cholesterol. Lipids and cholesterol were mixed together in chloroform to a final volume and concentration of 10 ml and  $10 \text{ mg}\cdot\text{ml}^{-1}$  respectively. This organic solution was evaporated to dryness in a Buchi Rotavapor Model R-114 (Buchi). This was resuspended in 10 ml of 0.1 mM EGTA and 50 mM Tris/HCl (pH 7.4). The suspension was freeze thawed at least 10 times using liquid nitrogen. The rehydrated lipid was put through a LIPEX extruder 11 times (Northern Lipids) with a 400 nm cutoff Millipore filter (EMD Millipore). Approximately  $100 \mu\text{M}$  of Pgp was dialysed against HEPES buffer (20 mM HEPES, 100 mM sodium chloride, 5 mM magnesium chloride, 2 mM DTT, pH 7.4) for 2 h to remove residual detergent. Then  $50 \mu\text{M}$  of dialysed protein and  $4 \text{ mg}\cdot\text{ml}^{-1}$  liposomes were incubated for 1 h. This was then dialysed for another 2 h against HEPES buffer to promote integration of the protein into the liposomes. To remove aggregated Pgp, the reconstituted liposomes were centrifuged for 5 min at 100 g in a Sorvall Legend Micro 21 centrifuge (ThermoScientific). To determine the orientation of mouse Pgp in the liposomes, the permeability of the reconstituted liposomes was tested with CHAPS detergent to expose nucleotide-binding domains (NBDs) oriented within the liposome [20,44,45]. Since there was no increase in the ATPase activity with increasing CHAPS concentrations, Pgp was assumed to be in an inside-out orientation.

### ATPase activity measurements

The ATPase activity of the Pgp transporter was measured using the Chifflet method [46]. The method estimates the ATPase activity by measuring the concentration of free  $\text{P}_i$  after ATP hydrolysis

through the formation of a  $\text{P}_i$ -molybdenum complex, which produces a strong absorbance signal at 850 nm. The absorbance at 850 nm was measured on a 96-well plate in a FlexStation 3 spectrometer (Molecular Devices). The ATPase activity of verapamil and digoxin was measured with  $50 \text{ nM}$  Pgp in Chifflet buffer (150 mM ammonium chloride, 5 mM magnesium sulfate, 0.02 % w/v sodium azide, 50 mM Tris/HCl, 2 mM DTT, pH 7.4).

Traditionally, simple enzyme kinetics have been analysed using linear transformations such as the Lineweaver–Burk (double reciprocal), Hans–Woolf or Eadie–Hofstee plots [47,48]. However, these plots suffer from a lack of variable independence across the axes and biasing of the error and the data points [49–51]. These methods have generally been superseded by non-linear regression methods that are significantly more accurate and no longer computationally inaccessible [50]. Therefore, for ATP hydrolysis kinetics that were monophasic, the ATP hydrolysis rate ( $v$ ), the maximum ATP hydrolysis rate ( $V_{\text{MAX}}$ ), the basal ATPase hydrolysis rate ( $v_{\text{basal}}$ ) and the Michaelis–Menten constant ( $K_m$ ) were estimated with the Michaelis–Menten equation (eqn 1) [48,52]:

$$v = \frac{V_{\text{MAX}} [L]}{K_m + [L]} + v_{\text{basal}} \quad (1)$$

For ATP hydrolysis kinetic curves showing biphasic substrate inhibition, the  $V_{\text{MAX}}$ ,  $K_m$  and the inhibitory constant ( $K_i$ ) were estimated with eqn (2) [48,52]:

$$v = \frac{V_{\text{MAX}}}{1 + \frac{K_m}{[L]} + \frac{[L]}{K_i}} + v_{\text{basal}} \quad (2)$$

For more complicated kinetics, fitting equations have been developed in some cases, but may require specialized numerical methods to solve and may result in multiple solutions [53].

To overcome these challenges, a variety of advanced software modelling packages have been developed to fit arbitrary kinetic models including the free complex pathway simulator (COPASI) [54] and the proprietary Berkeley Madonna (University of California, Berkeley, CA). For ATP hydrolysis kinetics observed in the presence of both verapamil and digoxin, the ATPase activity curves were fit to kinetic models using the evolutionary programming fitting algorithm in the COPASI software [54].

### Fluorescence spectroscopy

Quenching of intrinsic protein fluorescence has been used to measure the binding affinity of a chemically-diverse range of ligands with Pgp [55,56]. Drug-induced quenching of protein fluorescence with Pgp reconstituted in liposomes was investigated on an Olis DM 45 spectrofluorimeter (Olis Corp). All fluorescence samples contained  $1 \mu\text{M}$  liposome-reconstituted Pgp in Chifflet buffer (pH 7.4). Fluorescence emission was measured at 333 nm following excitation between 260 and 295 nm to minimize inner filter effects and background fluorescence. Drug-induced fluorescence quenching was corrected ( $F_{\text{corrected}}$ ) for background

fluorescence, dilution and inner filter effects with eqn (3) [57]:

$$F_{\text{corrected}} = (F - B) 10^{\frac{(\epsilon_{\text{ex}} b_{\text{ex}} + \epsilon_{\text{em}} b_{\text{em}}) [Q]}{2}} \quad (3)$$

where  $F$  is the measured protein fluorescence,  $B$  is the background and  $[Q]$  is the quenching ligand concentration. The molar absorption coefficients ( $\epsilon$ ) for excitation and emission are  $\epsilon_{\text{ex}}$  and  $\epsilon_{\text{em}}$  respectively. Verapamil was transparent above 300 nm and had  $\epsilon_{280 \text{ nm}}$  and  $\epsilon_{295 \text{ nm}}$  of 4 and  $0.27 \text{ mM}^{-1} \cdot \text{cm}^{-1}$  respectively. Digoxin was transparent above 250 nm. The pathlength ( $b$ ) along the excitation and emission axes are  $b_{\text{ex}}$  and  $b_{\text{em}}$  respectively. Drug-induced quenching of protein fluorescence from complexation of the ligand to the protein is known as static quenching, and can be used to estimate the drug's affinity. Drug-induced fluorescence quenching from random collisions with the protein is known as dynamic quenching [57]. Regardless of the nature of the quenching, the fluorescence quenching curves were fit to eqn (4) [57]:

$$F_{\text{corrected}} = \frac{F_{\text{corrected},0}}{1 + K [Q]} \quad (4)$$

where  $F_{\text{corrected},0}$  is the protein fluorescence in the absence of a quenching ligand and  $K$  is the association constant ( $K_A$ ) or the Stern–Volmer quenching constant ( $K_{\text{SV}}$ ) in the case of a static and dynamic quenching processes respectively. The two different quenching mechanisms can be differentiated by measuring the protein's fluorescence life time in the presence of the quenching ligand or by performing the fluorescence titration experiments at two different temperatures [57]. In the latter case, the  $K$  will increase with increasing temperature for dynamic quenching by increasing the collisional frequency of the quencher and will decrease in the case of static quenching by decreasing the residence time of the quenching ligand.

Acrylamide is a neutral aqueous collisional quencher that has been widely used to probe the accessibility of tryptophans in proteins and probe changes in tertiary structure [55,58]. Dynamic quenching of intrinsic tryptophan fluorescence by acrylamide has been used to probe conformational changes of Pgp [55,58,59]. For these experiments, fluorescence emission with Pgp reconstituted in liposomes was measured at 333 nm following excitation at 295 nm. Control acrylamide titrations were performed in the presence of *N*-acetyl-L-tryptophanamide (NATA) to estimate the degree of non-specific quenching [55]. Fluorescence intensities were corrected for with eqn (3) [57]. To produce the Stern–Volmer plots, the  $F_{\text{corrected},0}/F_{\text{corrected}}$  was plotted as a function of the acrylamide concentration. The degree of dynamic tryptophan quenching was estimated from the slopes of the Stern–Volmer curves, which is related to  $K_{\text{SV}}$  by  $F_{\text{corrected},0}/F_{\text{corrected}} = 1 + K_{\text{SV}}[Q]$  [57].

## NMR

All NMR experiments with verapamil and digoxin  $^1\text{H}$  NMR spectra were performed on a 600 MHz Varian INOVA spectrometer at  $25^\circ\text{C}$  equipped with a 5 mm z-gradient  $^1\text{H}\{^{13}\text{C}/^{15}\text{N}\}$  cryoprobe.

The  $^1\text{H}$  NMR peaks were assigned using standard  $^1\text{H}$  1D and 2D NMR techniques. NMR spectra were analysed using the iNMR software (<http://www.inmr.net>) and Igor Pro 6.2 (Wavemetrics). The  $^1\text{H}$  NMR peak assignments for verapamil and digoxin are shown in Supplementary Figure S1 in the Supplementary Information and were essentially identical with previous  $^1\text{H}$  NMR peak assignments [60,61].

The saturation transfer difference (STD) NMR technique is a well-established method for probing ligand–protein interactions [62]. With this technique, the protein is selectively excited at a frequency outside of the ligand  $^1\text{H}$  NMR peaks, the saturation is transferred from the excited protein to the ligand through spin diffusion and the ligand STD NMR signal is observed [63]. However, in the case of liposomes reconstituted with Pgp, there will be significant interference because of saturation transfer between the liposome membrane and the drugs. This interference can be subtracted from the saturation transfer between the drug and the protein by the NMR technique called STDD [64–67]. The STDD NMR procedure for membrane proteins was performed as described in [68]. STDD NMR samples contained  $1 \mu\text{M}$  Pgp reconstituted into liposomes in 100 mM potassium phosphate buffer [80%  $^2\text{H}_2\text{O}$  (99.9%) and 20%  $\text{ddH}_2\text{O}$ , pH 7.4]. The STDD NMR experiments were performed with a double pulsed field gradient spin echo pulse sequence to suppress background water, a 2s train of 50 ms shaped saturation pulses to selectively excite the protein and a total relaxation delay of 5 s [63]. The number of transients collected for the on resonance and the off resonance spectra were 512. To minimize saturation transfer between the drugs and the liposomes, samples were selectively irradiated at a frequency of 10.5 ppm. Control experiments were performed under identical conditions with liposomes and the drugs. To produce the STDD NMR spectrum,  $^1\text{H}$  STD NMR spectrum of liposomes with drugs was subtracted from the  $^1\text{H}$  STD NMR spectrum of Pgp reconstituted in liposomes with drugs ( $\Delta I$ ). The STDD NMR subtraction procedure is demonstrated with verapamil in Supplementary Figure S2 in the Supplementary Information. The STDD amplification factor was calculated using the following equation based on the STD amplification factor (eqn 5) [63]:

$$\text{STDD amplification factor} = \frac{[L]}{[P]} \frac{\Delta I}{I_0} \quad (5)$$

where  $[P]$  is the protein concentration and  $I_0$  is the amplitude of the  $^1\text{H}$  NMR peaks in the absence of saturating pulses.

## RESULTS

### The effect of verapamil and digoxin on the Pgp-coupled ATPase activity

Figure 2 shows the mouse Pgp-coupled ATPase activity of Pgp with verapamil and digoxin. In the absence of drugs, Pgp had basal ATPase activity of  $512 \pm 151 \text{ nmol} \cdot \text{min}^{-1} \cdot \text{mg}^{-1}$  at saturating 3.2 mM ATP, which is in the range of basal activity rates observed in the literature between 0 [69] and 2600  $\text{nmol} \cdot \text{min}^{-1} \cdot \text{mg}^{-1}$  [70].

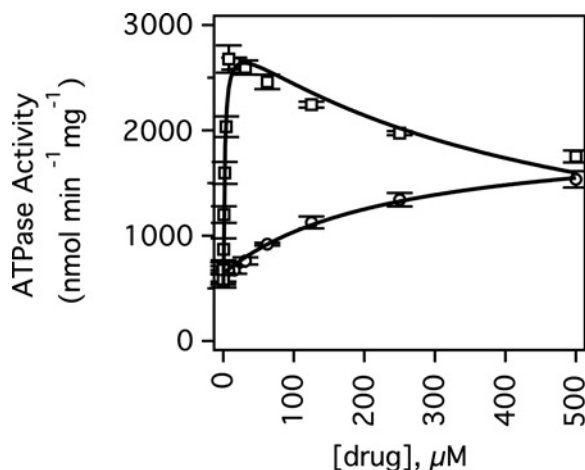


**Figure 2** Verapamil and digoxin-induced ATPase activation of Pgp

The Pgp-coupled ATPase activity as a function of verapamil (open squares) and digoxin (open circles) concentrations. The fits are shown as solid lines. Error bars represent the S.D. and the points represent an average of at least three independent experiments.

Kinetics of Pgp-coupled ATP hydrolysis in the presence of verapamil (Figure 2, open squares) was biphasic with substrate activation and inhibition of ATP hydrolysis reaching a maximum of  $2106 \pm 98 \text{ nmol} \cdot \text{min}^{-1} \cdot \text{mg}^{-1}$  or 3- to 4-fold activation at  $8 \mu\text{M}$  verapamil. Fitting the kinetics to the substrate inhibition equation (eqn 2) produced values for  $V_{\text{MAX}}$ ,  $K_m$  and  $K_i$  of  $2546 \pm 130 \text{ nmol} \cdot \text{min}^{-1} \cdot \text{mg}^{-1}$ ,  $1.9 \pm 0.5 \mu\text{M}$  and  $454 \pm 109 \mu\text{M}$  respectively. These results suggest that there is a high-affinity and a low-affinity verapamil-binding site on Pgp.

Biphasic verapamil kinetics with the transporter has been observed previously with hamster [70–73], human [20] and mouse [74] Pgp. These values are very similar to the average  $K_m$  and  $K_i$  values determined for mouse Pgp in Ehrlich membranes of 2.5 and  $225 \mu\text{M}$  [74] and for human Pgp in NIH-MDR1-G185 cells of 1.0 and  $843.6 \mu\text{M}$  respectively [20]. The  $V_{\text{MAX}}$  was also similar to previous determinations with mouse Pgp and the half maximal ATPase activity of  $4.2 \mu\text{M}$  with mouse Pgp was close to our estimates [39].

However, in a previous study [39], verapamil ATPase activation kinetics was monophasic and the maximum velocity was reached at  $150 \mu\text{M}$  rather than  $8 \mu\text{M}$ . Since the transporter is known to be sensitive to detergent and lipid composition [40,73,75–79], these differences in ATP hydrolysis kinetics were attributed to our procedure for reconstituting the transporter into the liposomes and our efforts to minimize the DDM during the protein purification process.

The digoxin-induced activation of ATP hydrolysis kinetics was monophasic and reached a maximum  $\sim 2$ -fold activation or  $\sim 1300 \text{ nmol} \cdot \text{min}^{-1} \cdot \text{mg}^{-1}$  (Figure 2, open circles), which is in the range observed previously [80–82]. The kinetics were fit to the Michaelis–Menten equation (eqn 1) and gave values for  $V_{\text{MAX}}$  and  $K_m$  of  $1344 \pm 149.8 \text{ nmol} \cdot \text{min}^{-1} \cdot \text{mg}^{-1}$  and  $240.4 \pm 68.1 \mu\text{M}$  respectively. This value is close to the  $K_m$  for digoxin transport

in human Pgp from Caco-2 cells of  $385 \mu\text{M}$  [83]. Although our  $K_m$  value was in the general range of previously determined  $K_m$  values for digoxin-induced ATPase activation of Pgp, the previously determined  $K_m$  values vary widely in the literature [80–82]. A  $K_m$  value of  $1.2 \mu\text{M}$  for ATPase activation by digoxin was determined in Caco-2 membrane vesicles containing human Pgp [80], whereas a  $K_m$  value of  $83.7 \mu\text{M}$  for ATPase activation was reported for human Pgp-enriched insect cell membranes [82]. For CR1R12 cells containing Pgp, maximal activation of ATP hydrolysis was not even reached at  $1000 \mu\text{M}$  digoxin [83] implying a  $K_m$  that is considerably higher than  $500 \mu\text{M}$ . This wide variation may be due to differences in membrane preparation, in lipid composition and/or in protein/lipid ratios.

### The effect of verapamil on the affinity of digoxin to Pgp by intrinsic protein fluorescence

Quenching of intrinsic protein fluorescence was used to probe the binding affinities of verapamil and digoxin to Pgp. Unfortunately, Pgp fluorescence at  $\sim 330 \text{ nm}$  was severely masked by inner filter effects and background fluorescence by verapamil when the protein was excited between 260 and 280 nm. Exciting the protein at 295 nm minimized these negative effects of verapamil on the protein fluorescence signal. Unlike previous studies with hamster Pgp [75], no significant verapamil-induced quenching of  $F_{\text{corrected}}$  was observed. However, this characteristic allowed us to examine the effects of verapamil on the affinity of digoxin to Pgp.

Figure 3 shows the effect of digoxin on the protein fluorescence of Pgp in the presence of low and high concentrations of verapamil. Pgp was most sensitive to protein fluorescence quenching by digoxin when the protein was excited at 280 nm. Figure 3A shows the effect of a range of digoxin concentrations on the uncorrected normalized protein fluorescence of Pgp after exciting at 280 nm. After correcting the fluorescence with eqn (3), the amplitude at 333 nm in panel A was plotted as a function of the digoxin concentration in Figure 3B and shows that Pgp is quenched  $\sim 10\%$  at saturating levels of digoxin. The titration curve appears to be monophasic with a  $K$  of  $0.0100 \pm 0.0018 \mu\text{M}^{-1}$  after fitting to eqn (4). To determine if the digoxin-induced quenching was due to a dynamic or a static quenching process, the titration was also performed at  $37^\circ\text{C}$ , which caused a decrease in the  $K$  value to  $0.0030 \pm 0.0008 \mu\text{M}^{-1}$  and showed that digoxin induced static quenching of Pgp. This allowed us to calculate a dissociation constant ( $K_D$ ) for digoxin binding to Pgp at  $25^\circ\text{C}$  of  $100 \pm 18 \mu\text{M}$  (i.e.  $K_A = 1/K_D$ ). A digoxin titration of Pgp was performed in the presence of  $8 \mu\text{M}$  verapamil, which caused the highest activation of Pgp-coupled ATP-hydrolysis in Figure 2 (closed squares). The  $F_{\text{corrected}}$  at 333 nm was plotted as a function of protein concentration and is shown in Figure 3C. A  $K_A$  value of  $0.0074 \pm 0.0033 \mu\text{M}^{-1}$  ( $K_D = 135 \pm 61 \mu\text{M}$ ) was extracted from fitting the curve, which was very similar to the value determined in the absence of verapamil implying that both verapamil and digoxin are bound simultaneously to Pgp. The verapamil concentration was increased to  $50 \mu\text{M}$  with the  $F_{\text{corrected}}$  digoxin titration shown

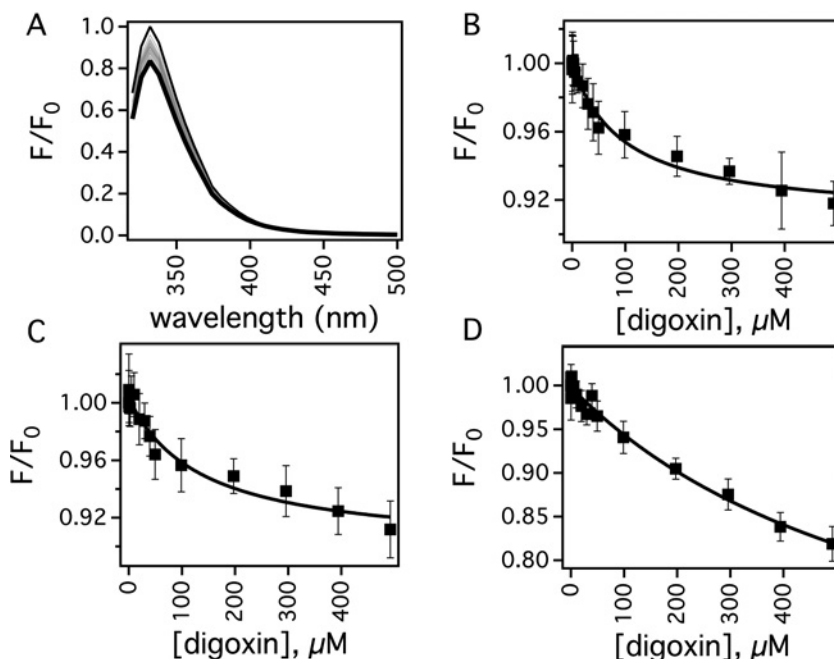


**Figure 3 Digoxin-induced fluorescence quenching of Pgp in the presence of verapamil at 25 °C**

(A) Pgp fluorescence spectra in the presence of a range of digoxin concentrations after exciting at 280 nm. The spectrum at 0 and 250  $\mu\text{M}$  digoxin are shown as thin and thick lines, respectively, whereas intermediate concentrations of digoxin are shown as grey lines. Protein fluorescence emission at 333 nm as a function of digoxin concentration and in the presence of (B) 0  $\mu\text{M}$ , (C) 8  $\mu\text{M}$  and (D) 50  $\mu\text{M}$  verapamil. The average and S.D. are represented as points and bars, respectively, and reflect at least three independent experiments.

in Figure 3D. The  $K_A$  determined by fitting this fluorescence quenching curve was  $0.0015 \pm 0.00057 \mu\text{M}^{-1}$  ( $K_D = 679 \pm 261 \mu\text{M}$ ). This is significantly lower than the  $K_A$  value determined at 8  $\mu\text{M}$  and 0  $\mu\text{M}$  verapamil. The decrease in  $K_A$  suggest that verapamil and digoxin are competitive at higher verapamil concentrations and that there is overlap in their binding sites. Digoxin titrations at higher verapamil concentrations with Pgp were attempted, but suffered from significant interference from inner filter effects by and fluorescence from verapamil (results not shown).

### Drug-induced conformational changes of Pgp by verapamil and digoxin

Acrylamide quenching of tryptophan fluorescence in the presence of drugs was used to investigate drug-induced conformational changes of Pgp. Figure 4 shows Stern–Volmer plots (i.e.  $F_0/F$  compared with [acrylamide]) in the absence and presence of drugs to probe protein conformational changes and tryptophan accessibility. The slope of the Stern–Volmer plot for Pgp in the absence of drugs had a  $K_{SV}$  value of  $1.55 \pm 0.04 \text{ M}^{-1}$  (Figure 4A, closed squares). The slope of the Stern–Volmer plot with NATA (Figure 4A, open squares) was measured to determine non-specific tryptophan interactions, and had a relatively high  $K_{SV}$  value of  $15.14 \pm 0.57 \text{ M}^{-1}$  that showed most of the tryptophans of Pgp are inaccessible to acrylamide. Figures 4B and 4C show the Stern–Volmer plots of Pgp in the presence of low and

high concentrations of verapamil.  $K_{SV}$  values of  $3.06 \pm 0.21 \text{ M}^{-1}$  and  $3.81 \pm 0.26 \text{ M}^{-1}$  were determined from the slopes of the plots with low and high concentrations of verapamil respectively. These differences show that verapamil shifts Pgp into at least two distinct conformations and the largest conformational changes occur at low concentrations of verapamil. This observation is consistent with verapamil-induced Pgp conformational changes deduced from cross-linking of [84–86], trypsin digestion of [87] and antibody competition with Pgp [88]. The slope of the Stern–Volmer plot for Pgp in the presence of 250  $\mu\text{M}$  digoxin was  $2.29 \pm 0.12 \text{ M}^{-1}$  (Figure 4D). When 8  $\mu\text{M}$  of verapamil was added to 250  $\mu\text{M}$  digoxin (Figure 4E), the  $K_{SV}$  value increased to  $3.44 \pm 0.19 \text{ M}^{-1}$ . Addition of high concentrations of verapamil to Pgp in the presence of 250  $\mu\text{M}$  digoxin increased the slope of the Stern–Volmer plot to  $3.87 \pm 0.26 \text{ M}^{-1}$  (Figure 4F), which is similar to the  $K_{SV}$  value determined from Figure 4C without digoxin and implies that they are in a similar conformation.

### Interactions of verapamil and digoxin with Pgp determined by STDD NMR

STDD NMR was used to probe the interactions of verapamil and digoxin with Pgp. Figure 5 shows the STDD NMR of verapamil and digoxin with Pgp. Figures 5A and 5B show the STDD NMR spectrum and amplification factors, respectively, with 1 mM verapamil and 1  $\mu\text{M}$  Pgp. Overall, the strongest interactions with Pgp occurred with the aromatic and methoxy

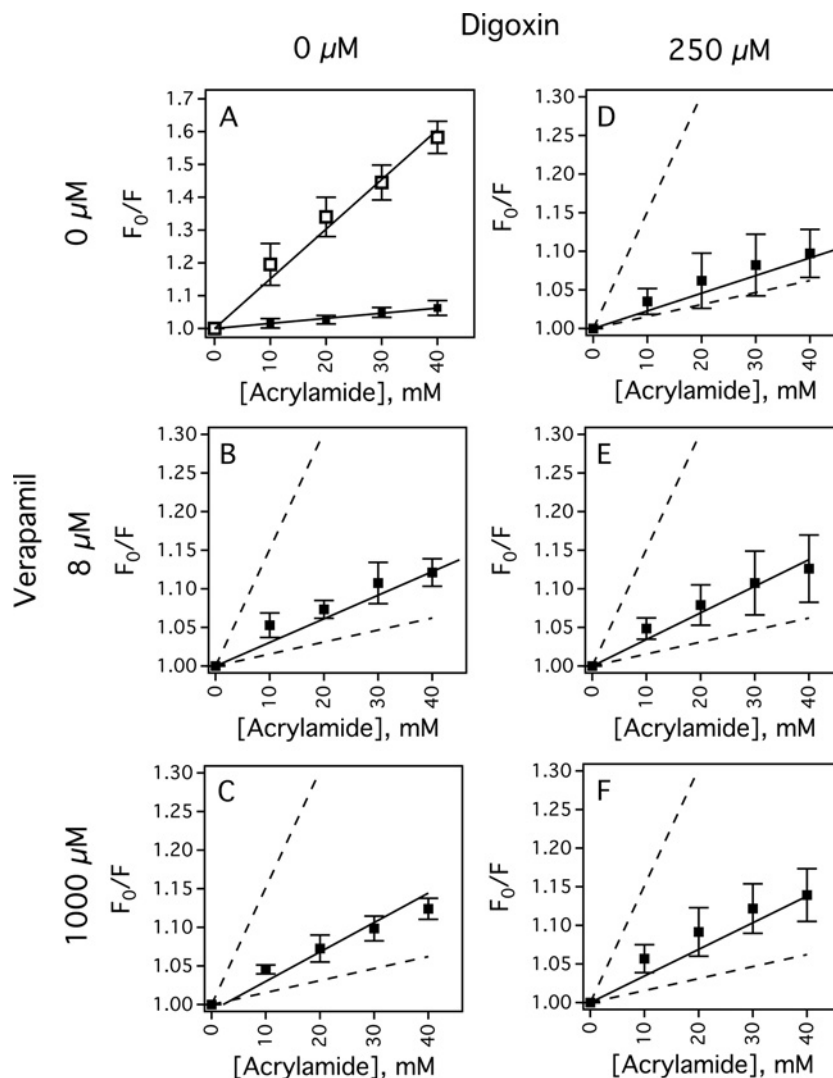


**Figure 4** Acrylamide quenching of the Pgp transporter in the presence of verapamil and digoxin

(A) The Stern–Volmer plots of NATA (open squares) and Pgp in the absence of drugs (closed squares). The Stern–Volmer plots of Pgp in the presence of (B and E) 8  $\mu\text{M}$  and (C and F) 1000  $\mu\text{M}$  verapamil. (D–F) The Stern–Volmer plots of Pgp with 250  $\mu\text{M}$  digoxin added in addition to verapamil. For comparison, the slopes in panel (A) are presented as dashed lines in panels (B) through (F). The average and S.D. are represented as points and bars, respectively, and reflect at least three independent experiments.

groups of verapamil with an STDD amplification factor of  $\sim 15$  indicating that they are the most important functional groups for molecular recognition by Pgp. STDD amplification factors that were half of these groups were observed for the methyls labelled A, A' and Q with STDD amplification factors of  $\sim 7$ . There were some weak STDD signals observed from the alkyl group (labelled L) of the distal phenyl group. No  $^1\text{H}$  STDD NMR peaks were observed for the other protons labelled G, H, I and K.

Figures 5C and 5D show the STDD NMR spectrum and amplification factors of 250  $\mu\text{M}$  digoxin with Pgp. Significant STDD NMR peaks were observed for several protons (e.g. 1''') emanating from the sugars and proton from the furan-2-one functional

group. The highest STDD amplification factor was observed for the proton that is near the 1,4  $\beta$ -linkage with an STDD amplification factor of  $\sim 8$ . To investigate the effect of verapamil on the interactions of digoxin with the transporter, 8  $\mu\text{M}$  of verapamil was added to samples containing protein and 250  $\mu\text{M}$  digoxin in Figures 5E and 5F. Because of the low verapamil concentration, no STDD NMR peaks were observed for this drug. The relative amplitudes of the STDD NMR spectrum were quite similar to the STDD NMR spectrum taken without 8  $\mu\text{M}$  verapamil. Therefore, low concentrations of verapamil did not significantly perturb digoxin's bound orientation to Pgp. However, the absolute amplitudes of the STDD NMR spectrum and amplification factors decreased  $\sim 50\%$  in the presence of 8  $\mu\text{M}$  verapamil.

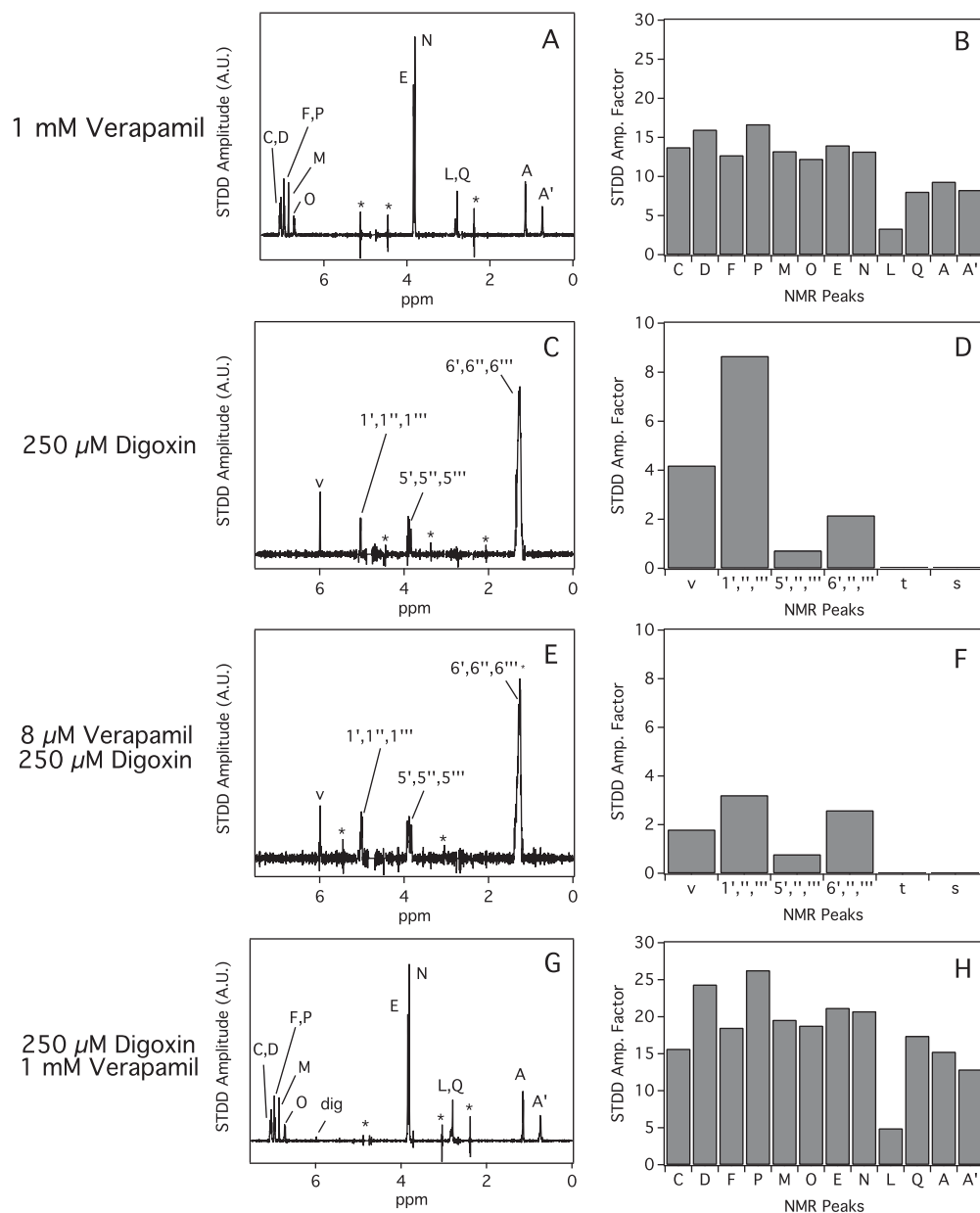


**Figure 5** STDD NMR of verapamil and digoxin with 1  $\mu$ M Pgp

The STDD amplification (amp.) factors were calculated from the STDD NMR spectra (**A**, **C**, **E** and **G**) for verapamil (**B** and **H**) and digoxin (**D** and **F**). The concentrations of verapamil and digoxin are shown on the left side of the figure. Parameters for the NMR experiments are in the 'Experimental' section.

This decrease was attributed to a fraction of verapamil molecules competing with digoxin bound to Pgp and to small errors in measuring the drug/protein ratios. The effect of higher concentrations of verapamil on digoxin's interaction with Pgp is shown in Figures 5G and 5H. No digoxin STDD NMR peaks were observed in the STDD NMR spectrum, which indicates complete displacement of digoxin from Pgp. The STDD amplification factors of verapamil were very similar to the  $^1\text{H}$  STDD NMR spectrum without digoxin (Figure 5A).

### Modelling Pgp-coupled ATPase activity with a panel of digoxin and verapamil concentrations

Figure 6 shows a DDI model and Pgp-coupled ATPase activity curves with a panel of digoxin and verapamil concentrations. The model shown in Figure 6A was the simplest that encompassed the results of the ATPase activity, intrinsic tryptophan fluorescence and the STDD NMR experiments. In the model, two verapamil molecules bind to Pgp, which is consistent with the biphasic ATP hydrolysis kinetics shown in Figure 2. The model also shows



that verapamil and digoxin bind simultaneously to Pgp (i.e. the enzyme verapamil-digoxin complex (EVD)). This is supported by the fact that the digoxin  $K_D$  is not significantly perturbed at low concentrations of verapamil and is also consistent with non-competitive inhibition for digoxin transport by verapamil [36,37]. In the model, higher concentrations of verapamil competitively displaces digoxin from its binding site on Pgp. Competitive displacement of digoxin by verapamil was observed at 50  $\mu\text{M}$  verapamil in the intrinsic tryptophan measurements of Pgp (Figure 3D). It was also demonstrated in the STDD NMR spectrum in Figure 5G by a lack of  $^1\text{H}$  digoxin STDD NMR peaks.

Figures 6B and 6C shows the Pgp ATPase activity with a range of digoxin and verapamil concentrations. Because of the complexity of the model shown in Figure 6A, the kinetics curves in Figures 6B and 6C were fit using the COPASI software package. A complete list of kinetic and thermodynamic parameters used to fit the curves in the figures is presented in Supplementary Table S1 of the Supplementary Information. The fits to the ATPase activity kinetic curves had correlations ( $R$ ) that were 0.9 or greater with one exception, which had a low  $\chi^2$ . The average basal ATP hydrolysis activity ( $V_{\text{MAX}0}$ ) determined from the fits was  $538 \pm 64 \text{ nmol}\cdot\text{min}^{-1}\cdot\text{mg}^{-1}$ .

Figure 6B shows the effect of digoxin on the ATPase activity with a range of verapamil concentrations. In the absence of digoxin,  $K_{D1}$ ,  $K_{D2}$ ,  $V_{\text{MAX}1}$  and  $V_{\text{MAX}2}$  values of 1.83  $\mu\text{M}$ , 211  $\mu\text{M}$ , 3000  $\text{nmol}\cdot\text{min}^{-1}\cdot\text{mg}^{-1}$  and 1100  $\text{nmol}\cdot\text{min}^{-1}\cdot\text{mg}^{-1}$ , respectively, for verapamil-induced activation of Pgp-coupled ATP hydrolysis were extracted from the fits. These dissociation constants were very similar to those obtained by fitting the ATPase activity kinetics curve in Figure 2 (open squares). Fitting all of the curves gave an average  $K_{D1}$ ,  $K_{D2}$ ,  $V_{\text{MAX}1}$  and  $V_{\text{MAX}2}$  for verapamil-induced activation of Pgp-coupled ATP hydrolysis of  $1.95 \pm 0.89 \mu\text{M}$ ,  $187 \pm 41 \mu\text{M}$ ,  $2757 \pm 313 \text{ nmol}\cdot\text{min}^{-1}\cdot\text{mg}^{-1}$  and  $896 \pm 132 \text{ nmol}\cdot\text{min}^{-1}\cdot\text{mg}^{-1}$  respectively.

Figure 6C shows the effect of verapamil on the ATPase activity with a range of digoxin concentrations. In the absence of verapamil, the ATPase activity kinetics with digoxin was monophasic and fits well to the model in Figure 6A with a  $K_{D3}$  and  $V_{\text{MAX}3}$  of 239  $\mu\text{M}$  and  $1983 \text{ nmol}\cdot\text{min}^{-1}\cdot\text{mg}^{-1}$ , which is similar to the  $K_D$  and  $V_{\text{MAX}}$  values obtained from fitting Figure 2 (open circles). The average  $K_{D3}$  and  $V_{\text{MAX}3}$  values for digoxin-induced ATPase activation determined from fitting all the curves with COPASI were  $206 \pm 53 \mu\text{M}$  and  $1981 \pm 207 \text{ nmol}\cdot\text{min}^{-1}\cdot\text{mg}^{-1}$ .

The remaining parameters were estimated indirectly by fitting with COPASI. The affinity of digoxin to Pgp in the presence of verapamil ( $K_{D4}$ ) was  $292 \pm 89 \mu\text{M}$ . This is very similar to the  $K_{D2}$  determined in the absence of verapamil. The affinity of verapamil to Pgp in the presence of digoxin ( $K_{D5}$ ) was  $3.41 \pm 1.91 \mu\text{M}$ , which is relatively close to  $K_{D1}$ . These results suggest that verapamil and digoxin were essentially not cooperative with respect to binding to Pgp. The  $V_{\text{MAX}4,5}$  for drug-induced ATPase activation from simultaneous binding of digoxin and verapamil was  $121 \pm 139 \text{ nmol}\cdot\text{min}^{-1}\cdot\text{mg}^{-1}$  and reflects an almost complete inhibition of ATP hydrolysis in the presence of both drugs. In this case, verapamil and digoxin are negatively cooperative with respect to Pgp-coupled ATP hydrolysis. This

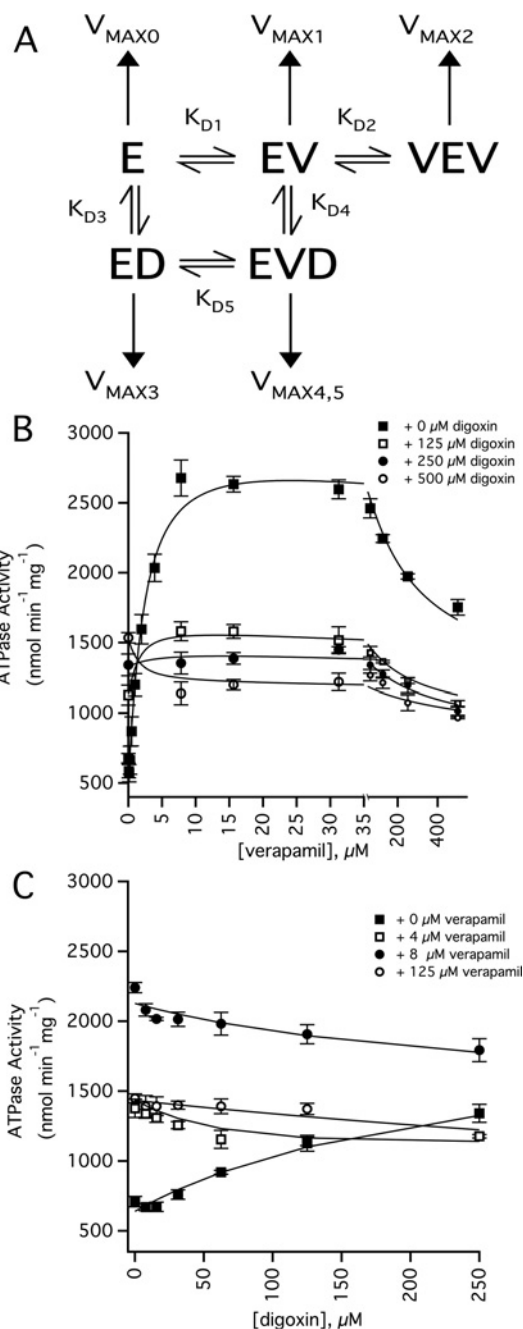


**Figure 6** DDI effects of verapamil and digoxin on the ATPase activity of Pgp

(A) DDI model used to fit the ATPase activity curves. Horizontal and vertical arrows denote the equilibria between bound states and the ATPase activity from the bound states respectively. E, V and D correspond to Pgp, verapamil and digoxin respectively. (B) Verapamil-induced activation of ATPase activity in the presence of 0  $\mu\text{M}$  (closed squares), 125  $\mu\text{M}$  (open squares), 250  $\mu\text{M}$  (closed circles) and 500  $\mu\text{M}$  digoxin (open circles). (C) Digoxin-induced activation of ATPase activity in the presence of 0  $\mu\text{M}$  (closed squares), 4  $\mu\text{M}$  (open squares), 8  $\mu\text{M}$  (closed circles) and 125  $\mu\text{M}$  verapamil (open circles). The fits are shown as lines, the error bars represent the S.D. and the points represent an average of at least three independent experiments. The statistics and the values used to fit the curves are shown in Supplementary Table S1 of the Supplementary Information.

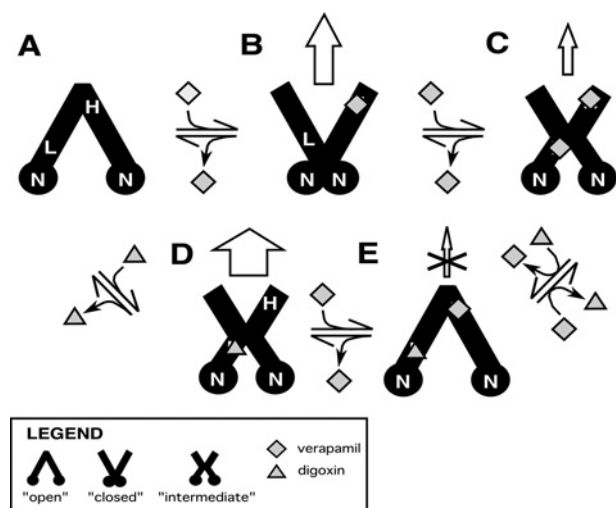


**Figure 7 DDI transport model of verapamil and digoxin with Pgp**

Pgp is shown as a cartoon representation of three conformational states: ‘open’, ‘closed’ and ‘intermediate’. Verapamil and digoxin are represented as diamonds and triangles respectively. The panels show Pgp (A) in the absence of drugs, (B) with 1 bound verapamil molecule, (C) with 2 bound verapamil molecules, (D) with 1 digoxin molecule bound and (E) with 1 bound verapamil and 1 bound digoxin. The top and the bottom of the Pgp representations are the extracellular and cytosolic sides respectively. The vertical arrows denote transport and the size of the arrows reflect their relative transport rates, whereas X denotes transport inhibition. H, L and N are the high-affinity binding site, low-affinity binding site and the NBDs respectively.

also correlates well with non-competitive inhibition of digoxin transport by Pgp in the presence of verapamil [36,37].

## DISCUSSION

In Figure 7, we propose a DDI transport model with Pgp based on our results with verapamil and digoxin, and the conformational changes that Pgp is known to undergo with nucleotide cofactors and drugs [85,86,89,90]. For simplicity, we have represented Pgp in our model by three conformations: ‘open’, ‘closed’ and ‘intermediate’. In reality, these conformations represent an ensemble average between a range of conformations. In the ‘open’ conformation, the NBDs are relatively far apart and the cytosolic side is exposed to the bulk solvent. In the ‘closed’ conformation, the NBDs are in contact with each other and the extracellular side is exposed to the bulk solvent. The ‘intermediate’ conformation is between the ‘open’ and ‘closed’ conformations. In this conformation, both the cytosolic and extracellular sides of Pgp are exposed to the bulk solvent.

Drug-induced changes in tryptophan accessibility deduced from the acrylamide quenching experiments implied that Pgp occupies distinct conformations at each of the digoxin and verapamil concentrations. Unfortunately, this information cannot be used to assign specific drug-bound Pgp conformations. Instead, the assignment was based on drug-induced activation of the Pgp-coupled ATP hydrolysis rate. Our rationale was based on

the fact that site-directed mutagenesis and cross-linking studies of Pgp in addition to structural studies of the bacterial transporters with nucleotide analogues have demonstrated that the interaction of the Pgp nucleotide domains with each other is essential for ATP hydrolysis [86,91–96]. Therefore, the average distance between the NBDs of Pgp was correlated to the ATP hydrolysis rate in our model. In other words, drugs that induce a relatively low and high ATPase rates will shift Pgp into ‘open’ and ‘closed’ conformations respectively.

The locations of the verapamil-binding sites are currently unknown. The biphasic verapamil ATPase activation kinetics that are shown in Figures 2 and 6 suggest a high- and a low-affinity verapamil-binding site on Pgp. Several studies have identified residues clustered near the extracellular side of Pgp [97–99] and G185 [100,101], which lies in the transmembrane region of Pgp, that have marked effects on verapamil-induced activation of ATP hydrolysis and transport. Deletion of residues between 78 and 97 near the extracellular side of human Pgp caused a dramatic increase in the  $K_m$  for ATPase activation by verapamil [97]. Multiple mutations near the extracellular side of human Pgp decreased activity towards verapamil transport [99]. Permanent ATPase activation of human Pgp was observed in cysteineless human Pgp with an I306C mutation labelled with a thiol-reactive verapamil analogue [98]. Mutating the G185 residue had very strong effects on the  $V_{MAX}$  of verapamil-induced ATPase activation [100,101]. The mutation also had significant effects on the  $K_i$  for substrate inhibition for verapamil, but negligible effects on verapamil’s  $K_m$  [100]. By affecting the  $K_i$  and not the  $K_m$  suggested to us that the mutation is affecting an alternate verapamil-binding site. With this information, the high-affinity (H) drug-binding site is placed roughly near the extracellular side of Pgp, whereas the low-affinity (L) drug-binding site is closer to the NBDs within the transmembrane region of the transporter in Figure 7A.

Figure 7A shows Pgp in the absence of ligands. Because the ATPase hydrolysis rate in the absence of ligands is relatively low at  $\sim 500 \text{ nmol}\cdot\text{min}^{-1}\cdot\text{mg}^{-1}$ , Pgp will be in an ‘open’ conformation with the NBDs (N) separated in our model.

At low verapamil concentrations, the drug binds to the H site in Figure 7B. Fitting the Pgp-coupled ATPase activity kinetics of Figure 6B gave a  $V_{MAX}$  of  $\sim 3000 \text{ nmol}\cdot\text{min}^{-1}\cdot\text{mg}^{-1}$ . This is the highest ATPase activation observed for either drug. Therefore, Pgp is proposed to be in the ‘closed’ conformation under these conditions.

At higher verapamil concentrations, the drug will occupy the L site on Pgp in Figure 7C. The degree of ATPase activation is less than half the Pgp-coupled ATPase activation at lower verapamil concentrations, but is significantly higher than basal Pgp-coupled ATPase activity. Therefore, Pgp is proposed to be in an intermediate conformation. Consistent with the concentration-dependence observed for ATPase activation by verapamil, the drug transport rate is also concentration-dependent. In Caco-2 cells containing human Pgp, verapamil had a higher permeability ratio with Pgp at low opposed to higher verapamil concentrations [23]. Also, human Pgp overexpressed in LLC-PK1 cells had higher efflux ratios at 350 nM than 5  $\mu\text{M}$  verapamil [21,25]. Therefore, we propose that verapamil occupancy at the H site

alone (Figure 7B) will lead to higher verapamil transport rates than occupancy at both drug-binding sites (Figure 7C).

Addition of digoxin leads to formation of the Pgp complex shown in Figure 7D. The affinities deduced from the intrinsic protein fluorescence (Figure 3) and from fitting the ATPase activity kinetics curves (Figures 2 and 6) posits the drug in the L site. The degree of Pgp-coupled ATPase activation by digoxin was similar to the Pgp-coupled ATPase activation in the presence of high concentrations of verapamil. The relative tryptophan accessibility determined from the slopes of the Stern–Volmer plots was similar under both of these conditions (cf. Figures 4E and 4C). Therefore, Pgp will be in an intermediate conformation in our model. The permeability/efflux ratios of digoxin with Pgp in several cell lines ranged between 4 and 35 [21,24,102,103]. This contrasts with the permeability/efflux ratios for Pgp at low verapamil concentrations, which were generally lower and ranged from ~1 to 6 [21,23,24]. These results suggest that the coupling between ATP hydrolysis and transport for drugs may be ligand dependent.

When low verapamil concentrations are added to the digoxin–Pgp complex, verapamil will occupy the H site and form the complex shown in Figure 7E. Several lines of evidence support the simultaneous binding of verapamil and digoxin to Pgp. First, verapamil non-competitively inhibits digoxin transport by Pgp [36,37]. Second, the  $K_D$ s determined from fitting the intrinsic protein fluorescence quenching curves in Figure 3 showed that addition of low concentrations of verapamil does not significantly change the  $K_D$  of digoxin to Pgp. Third, there are significant  $^1\text{H}$  STDD NMR peaks for digoxin at 8  $\mu\text{M}$  verapamil (Figure 5E), which is a high enough verapamil concentration to saturate the H site. Fitting the Pgp-coupled ATPase activity curves in Figure 6 revealed that binding of both drugs will inhibit ATP hydrolysis. Therefore, Pgp will be in the ‘open’ conformation.

Higher concentrations of verapamil will completely displace digoxin from the L site forming the double bound complex in Figure 7C. This configuration is supported by our results that showed the affinity decreased significantly at verapamil concentrations above 8  $\mu\text{M}$  (Figure 3). This is also supported by the complete loss of  $^1\text{H}$  STDD NMR signals from digoxin in the presence of 1 mM verapamil (Figure 5G) and implied by the similarity of the Stern–Volmer plots of Pgp with 1 mM verapamil in the absence and presence of 250  $\mu\text{M}$  digoxin (cf. Figures 4C and 4F).

#### AUTHOR CONTRIBUTION

Arthur Roberts and Kaitlyn Ledwitch conceived and coordinated the study and wrote the paper. Arthur Roberts and Kaitlyn Ledwitch designed the experiments for all the figures. Kaitlyn Ledwitch prepared the figures. Kaitlyn Ledwitch performed and analysed the experiments for all the figures. Robert Barnes collected fluorescence data for Figures 3 and 4. Robert Barnes also did some of the proteoliposome preparations for these studies. All the authors approved the final version of the manuscript.

#### ACKNOWLEDGEMENTS

We thank Dr Ina L. Urbatsch of Texas Tech University Health Sciences Center for her generous gift of *P. pastoris* with the wild-type

mouse Pgp transporter gene. We also thank her postdoc Dr Douglas J. Swartz for sending us the materials and providing protocols for genetically manipulating and purifying Pgp from *P. pastoris* for our laboratory. Without their contribution and generosity, this research would not be possible.

#### FUNDING

This work was supported by the American Heart Association Grant [grant number 14GRNT20450044]; and the National Institute of Health [grant number 1R15GM107913-01A1].

#### REFERENCES

- Bailey, D.G. and Dresser, G.K. (2004) Interactions between grapefruit juice and cardiovascular drugs. *Am. J. Cardiovasc. Drugs* **4**, 281–297 [CrossRef PubMed](#)
- Lattuca, B., Khoueiry, Z., Malcles, G., Davy, J.M. and Leclercq, F. (2013) Drug interactions between non-steroidal anti-inflammatory drugs and cardiovascular treatments (except anti-agregant therapy). *Antiinflamm. Antiallergy Agents Med. Chem.* **12**, 36–46 [CrossRef PubMed](#)
- Mateti, U.V., Rajakannan, T., Nekkanti, H., Rajesh, V., Mallaysamy, S.R. and Ramachandran, P. (2011) Drug–drug interactions in hospitalized cardiac patients. *J. Young Pharm.* **3**, 329–333 [CrossRef PubMed](#)
- Mendell, J., Zahir, H., Matsushima, N., Noveck, R., Lee, F., Chen, S., Zhang, G. and Shi, M. (2013) Drug–drug interaction studies of cardiovascular drugs involving P-glycoprotein, an efflux transporter, on the pharmacokinetics of edoxaban, an oral factor Xa inhibitor. *Am. J. Cardiovasc. Drugs* **13**, 331–342 [CrossRef PubMed](#)
- Zaidenstein, R., Eyal, S., Efrati, S., Akivison, L., Michowitz, M.K., Nagornov, V. and Golik, A. (2002) Adverse drug events in hospitalized patients treated with cardiovascular drugs and anticoagulants. *Pharmacoepidemiol. Drug Saf.* **11**, 235–238 [CrossRef PubMed](#)
- Seelig, A. (1998) A general pattern for substrate recognition by P-glycoprotein. *Eur. J. Biochem.* **251**, 252–261 [CrossRef PubMed](#)
- Wessler, J.D., Grip, L.T., Mendell, J. and Giugliano, R.P. (2013) The P-glycoprotein transport system and cardiovascular drugs. *J. Am. Coll. Cardiol.* **61**, 2495–2502 [CrossRef PubMed](#)
- Lum, B.L. and Gosland, M.P. (1995) MDR expression in normal tissues. Pharmacologic implications for the clinical use of P-glycoprotein inhibitors. *Hematol. Oncol. Clin. North Am.* **9**, 319–336 [PubMed](#)
- Ceckova-Novotna, M., Pavek, P. and Staud, F. (2006) P-glycoprotein in the placenta: expression, localization, regulation and function. *Reprod. Toxicol.* **22**, 400–410 [CrossRef PubMed](#)
- Couture, L., Nash, J.A. and Turgeon, J. (2006) The ATP-binding cassette transporters and their implication in drug disposition: a special look at the heart. *Pharmacol. Rev.* **58**, 244–258 [CrossRef PubMed](#)
- Meissner, K., Sperker, B., Karsten, C., Meyer Zu Schwabedissen, H., Seeland, U., Bohm, M., Bien, S., Dazert, P., Kunert-Keil, C., Vogelgesang, S. et al. (2002) Expression and localization of P-glycoprotein in human heart: effects of cardiomyopathy. *J. Histochem. Cytochem.* **50**, 1351–1356 [CrossRef PubMed](#)
- Cascorbi, I., Paul, M. and Kroemer, H.K. (2004) Pharmacogenomics of heart failure – focus on drug disposition and action. *Cardiovasc. Res.* **64**, 32–39 [CrossRef PubMed](#)



- 13 Rodriguez, I., Abernethy, D.R. and Woosley, R.L. (1999) P-glycoprotein in clinical cardiology. *Circulation* **99**, 472–474 [CrossRef PubMed](#)
- 14 Marchetti, S., Mazzanti, R., Beijnen, J.H. and Schellens, J.H. (2007) Concise review: clinical relevance of drug drug and herb drug interactions mediated by the ABC transporter ABCB1 (MDR1, P-glycoprotein). *Oncologist* **12**, 927–941 [CrossRef PubMed](#)
- 15 Fleckenstein, A. (1977) Specific pharmacology of calcium in myocardium, cardiac pacemakers, and vascular smooth muscle. *Annu. Rev. Pharmacol. Toxicol.* **17**, 149–166 [CrossRef PubMed](#)
- 16 Gould, B.A., Mann, S., Kieso, H., Subramanian, V.B. and Raftery, E.B. (1982) The 24-hour ambulatory blood pressure profile with verapamil. *Circulation* **65**, 22–27 [CrossRef PubMed](#)
- 17 Lewis, G.R., Morley, K.D., Lewis, B.M. and Bones, P.J. (1978) The treatment of hypertension with verapamil. *N.Z. Med. J.* **87**, 351–354 [PubMed](#)
- 18 Lewis, G.R., Morley, K.D., Maslowski, A.H. and Bones, P.J. (1979) Verapamil in the management of hypertensive patients. *Aust. N.Z. J. Med.* **9**, 62–64 [CrossRef PubMed](#)
- 19 Neugebauer, G. (1978) Comparative cardiovascular actions of verapamil and its major metabolites in the anaesthetised dog. *Cardiovasc. Res.* **12**, 247–254 [CrossRef PubMed](#)
- 20 Aanismaa, P. and Seelig, A. (2007) P-glycoprotein kinetics measured in plasma membrane vesicles and living cells. *Biochemistry* **46**, 3394–3404 [CrossRef PubMed](#)
- 21 Schwab, D., Fischer, H., Tabatabaei, A., Poli, S. and Huwyler, J. (2003) Comparison of *in vitro* P-glycoprotein screening assays: recommendations for their use in drug discovery. *J. Med. Chem.* **46**, 1716–1725 [CrossRef PubMed](#)
- 22 Polli, J.W., Wring, S.A., Humphreys, J.E., Huang, L., Morgan, J.B., Webster, L.O. and Serabjit-Singh, C.S. (2001) Rational use of *in vitro* P-glycoprotein assays in drug discovery. *J. Pharmacol. Exp. Ther.* **299**, 620–628 [PubMed](#)
- 23 Faassen, F., Vogel, G., Spanings, H. and Vromans, H. (2003) Caco-2 permeability, P-glycoprotein transport ratios and brain penetration of heterocyclic drugs. *Int. J. Pharm.* **263**, 113–122 [CrossRef PubMed](#)
- 24 Haslam, I.S., Jones, K., Coleman, T. and Simmons, N.L. (2008) Induction of P-glycoprotein expression and function in human intestinal epithelial cells (T84). *Biochem. Pharmacol.* **76**, 850–861 [CrossRef PubMed](#)
- 25 Pauli-Magnus, C., von Richter, O., Burk, O., Ziegler, A., Mettang, T., Eichelbaum, M. and Fromm, M.F. (2000) Characterization of the major metabolites of verapamil as substrates and inhibitors of P-glycoprotein. *J. Pharmacol. Exp. Ther.* **293**, 376–382 [PubMed](#)
- 26 Mahar Doan, K.M., Humphreys, J.E., Webster, L.O., Wring, S.A., Shampine, L.J., Serabjit-Singh, C.J., Adkison, K.K. and Polli, J.W. (2002) Passive permeability and P-glycoprotein-mediated efflux differentiate central nervous system (CNS) and non-CNS marketed drugs. *J. Pharmacol. Exp. Ther.* **303**, 1029–1037 [CrossRef PubMed](#)
- 27 Romermann, K., Wanek, T., Bankstahl, M., Bankstahl, J.P., Fedowitz, M., Muller, M., Loscher, W., Kuntner, C. and Langer, O. (2013) (R)-[(11)C]verapamil is selectively transported by murine and human P-glycoprotein at the blood-brain barrier, and not by MRP1 and BCRP. *Nucl. Med. Biol.* **40**, 873–878 [CrossRef PubMed](#)
- 28 Cao, X., Yu, L.X., Barbaciru, C., Landowski, C.P., Shin, H.C., Gibbs, S., Miller, H.A., Amidon, G.L. and Sun, D. (2005) Permeability dominates *in vivo* intestinal absorption of P-gp substrate with high solubility and high permeability. *Mol. Pharm.* **2**, 329–340 [CrossRef PubMed](#)
- 29 Ke, A.B., Eyal, S., Chung, F.S., Link, J.M., Mankoff, D.A., Muzi, M. and Unadkat, J.D. (2013) Modeling cyclosporine A inhibition of the distribution of a P-glycoprotein PET ligand, 11C-verapamil, into the maternal brain and fetal liver of the pregnant nonhuman primate: impact of tissue blood flow and site of inhibition. *J. Nucl. Med.* **54**, 437–446 [CrossRef PubMed](#)
- 30 Litman, T., Zeuthen, T., Skovsgaard, T. and Stein, W.D. (1997) Competitive, non-competitive and cooperative interactions between substrates of P-glycoprotein as measured by its ATPase activity. *Biochim. Biophys. Acta* **1361**, 169–176 [CrossRef PubMed](#)
- 31 Klein, H.O., Lang, R., Weiss, E., Di Segni, E., Libhaber, C., Guerrero, J. and Kaplinsky, E. (1982) The influence of verapamil on serum digoxin concentration. *Circulation* **65**, 998–1003 [CrossRef PubMed](#)
- 32 Pedersen, K.E., Dorph-Pedersen, A., Hvidt, S., Klitgaard, N.A. and Pedersen, K.K. (1982) The long-term effect of verapamil on plasma digoxin concentration and renal digoxin clearance in healthy subjects. *Eur. J. Clin. Pharmacol.* **22**, 123–127 [CrossRef PubMed](#)
- 33 Ehle, M., Patel, C. and Giugliano, R.P. (2011) Digoxin: clinical highlights: a review of digoxin and its use in contemporary medicine. *Crit. Pathw. Cardiol.* **10**, 93–98 [CrossRef PubMed](#)
- 34 Englund, G., Hallberg, P., Artursson, P., Michaelsson, K. and Melhus, H. (2004) Association between the number of coadministered P-glycoprotein inhibitors and serum digoxin levels in patients on therapeutic drug monitoring. *BMC Med.* **2**, 8 [CrossRef PubMed](#)
- 35 Tanigawara, Y. (2000) Role of P-glycoprotein in drug disposition. *Ther. Drug Monit.* **22**, 137–140 [CrossRef PubMed](#)
- 36 Verschraagen, M., Koks, C.H., Schellens, J.H. and Beijnen, J.H. (1999) P-glycoprotein system as a determinant of drug interactions: the case of digoxin–verapamil. *Pharmacol. Res.* **40**, 301–306 [CrossRef PubMed](#)
- 37 Ito, S., Woodland, C., Harper, P.A. and Koren, G. (1993) The mechanism of the verapamil–digoxin interaction in renal tubular cells (LLC-PK1). *Life Sci.* **53**, PL399–PL403 [PubMed](#)
- 38 Gordon, M. and Goldenberg, L.M. (1986) Clinical digoxin toxicity in the aged in association with co-administered verapamil. A report of two cases and review of the literature. *J. Am. Geriatr. Soc.* **34**, 659–662 [CrossRef PubMed](#)
- 39 Bai, J., Swartz, D.J., Protasevich, I.I., Brouillette, C.G., Harrell, P.M., Hildebrandt, E., Gasser, B., Mattanovich, D., Ward, A., Chang, G. and Urbatsch, I.L. (2011) A gene optimization strategy that enhances production of fully functional P-glycoprotein in *Pichia pastoris*. *PLoS One* **6**, e22577 [CrossRef PubMed](#)
- 40 Lerner-Marmarosh, N., Gimi, K., Urbatsch, I.L., Gros, P. and Senior, A.E. (1999) Large scale purification of detergent-soluble P-glycoprotein from *Pichia pastoris* cells and characterization of nucleotide binding properties of wild-type, Walker A, and Walker B mutant proteins. *J. Biol. Chem.* **274**, 34711–34718 [CrossRef PubMed](#)
- 41 Dunn, B. and Wobbe, C.R. (2001) Preparation of protein extracts from yeast. *Curr. Protoc. Mol. Biol.* **Chapter 13**, Unit 13.13
- 42 Mui, B., Chow, L. and Hope, M.J. (2003) Extrusion technique to generate liposomes of defined size. *Methods Enzymol.* **367**, 3–14 [CrossRef PubMed](#)
- 43 Rigaud, J.L. and Levy, D. (2003) Reconstitution of membrane proteins into liposomes. *Methods Enzymol.* **372**, 65–86 [CrossRef PubMed](#)
- 44 Shapiro, A.B. and Ling, V. (1995) Reconstitution of drug transport by purified P-glycoprotein. *J. Biol. Chem.* **270**, 16167–16175 [CrossRef PubMed](#)
- 45 Sharom, F.J., Yu, X. and Doige, C.A. (1993) Functional reconstitution of drug transport and ATPase activity in proteoliposomes containing partially purified P-glycoprotein. *J. Biol. Chem.* **268**, 24197–24202 [PubMed](#)
- 46 Chifflet, S., Torriglia, A., Chiesa, R. and Tolosa, S. (1988) A method for the determination of inorganic phosphate in the presence of labile organic phosphate and high concentrations of protein: application to lens ATPases. *Anal. Biochem.* **168**, 1–4 [CrossRef PubMed](#)

- 47 Cook, P.F. and Cleland, W.W. (2007) Enzyme kinetics and mechanism, Garland Science, London, New York
- 48 Segel, I.H. (1975) Enzyme Kinetics: Behavior and Analysis of Rapid Equilibrium and Steady-State Enzyme Systems, John Wiley & Sons, Inc., New York
- 49 Martin, R.B. (1997) Disadvantages of double reciprocal plots. *J. Chem. Educ.* **74**, 1238 [CrossRef](#)
- 50 Leatherbarrow, R.J. (1990) Using linear and non-linear regression to fit biochemical data. *Trends Biochem. Sci.* **15**, 455–458 [CrossRef](#) [PubMed](#)
- 51 Ranaldi, F., Vanni, P. and Giachetti, E. (1999) What students must know about the determination of enzyme kinetic parameters. *Biochem. Educ.* **27**, 87–91 [CrossRef](#)
- 52 Roberts, A.G., Yang, J., Halpert, J.R., Nelson, S.D., Thummel, K.T. and Atkins, W.M. (2011) The structural basis for homotropic and heterotropic cooperativity of midazolam metabolism by human cytochrome P450 3A4. *Biochemistry* **50**, 10804–10818 [CrossRef](#) [PubMed](#)
- 53 Davydov, D.R., Botchkareva, A.E., Davydova, N.E. and Halpert, J.R. (2005) Resolution of two substrate-binding sites in an engineered cytochrome P450eryF bearing a fluorescent probe. *Biophys. J.* **89**, 418–432 [CrossRef](#) [PubMed](#)
- 54 Hoops, S., Sahle, S., Gauges, R., Lee, C., Pahle, J., Simus, N., Singhal, M., Xu, L., Mendes, P. and Kummer, U. (2006) COPASI – a COmplex PATHway Simulator. *Bioinformatics* **22**, 3067–3074 [CrossRef](#) [PubMed](#)
- 55 Liu, R., Siemiarz, A. and Sharom, F.J. (2000) Intrinsic fluorescence of the P-glycoprotein multidrug transporter: sensitivity of tryptophan residues to binding of drugs and nucleotides. *Biochemistry* **39**, 14927–14938 [CrossRef](#) [PubMed](#)
- 56 Sharom, F.J., Russell, P.L., Qu, Q. and Lu, P. (2003) Fluorescence techniques for studying membrane transport proteins: the P-glycoprotein multidrug transporter. *Methods Mol. Biol.* **227**, 109–128 [PubMed](#)
- 57 Lakowicz, J.R. (1999) Principles of Fluorescence Spectroscopy, Kluwer Academic/Plenum, New York [CrossRef](#)
- 58 Sonveaux, N., Viganò, C., Shapiro, A.B., Ling, V. and Ruysschaert, J.M. (1999) Ligand-mediated tertiary structure changes of reconstituted P-glycoprotein. A tryptophan fluorescence quenching analysis. *J. Biol. Chem.* **274**, 17649–17654 [CrossRef](#) [PubMed](#)
- 59 Russell, P.L. and Sharom, F.J. (2006) Conformational and functional characterization of trapped complexes of the P-glycoprotein multidrug transporter. *Biochem. J.* **399**, 315–323 [CrossRef](#) [PubMed](#)
- 60 Maccotta, A., Scibona, G., Valensin, G., Gaggelli, E., Botre, F. and Botre, C. (1991) Nuclear magnetic resonance investigations of calcium antagonist drugs. II: Conformational and dynamic features of verapamil in [2H<sub>6</sub>]DMSO. *J. Pharm. Sci.* **80**, 586–589 [CrossRef](#) [PubMed](#)
- 61 Tetreault, S. and Ananthanarayanan, V.S. (1993) Interaction of calcium channel antagonists with calcium: structural studies on verapamil and its Ca<sup>2+</sup> complex. *J. Med. Chem.* **36**, 1017–1023 [CrossRef](#) [PubMed](#)
- 62 Leach, A.R. and Hann, M.M. (2011) Molecular complexity and fragment-based drug discovery: ten years on. *Curr. Opin. Chem. Biol.* **15**, 489–496 [CrossRef](#) [PubMed](#)
- 63 Mayer, M. and Meyer, B. (2001) Group epitope mapping by saturation transfer difference NMR to identify segments of a ligand in direct contact with a protein receptor. *J. Am. Chem. Soc.* **123**, 6108–6117 [CrossRef](#) [PubMed](#)
- 64 Claasen, B., Axmann, M., Meinecke, R. and Meyer, B. (2005) Direct observation of ligand binding to membrane proteins in living cells by a saturation transfer double difference (STDD) NMR spectroscopy method shows a significantly higher affinity of integrin  $\alpha_{IIb}\beta_3$  in native platelets than in liposomes. *J. Am. Chem. Soc.* **127**, 916–919 [CrossRef](#) [PubMed](#)
- 65 Haselhorst, T., Munster-Kuhnel, A.K., Oschlies, M., Tiralongo, J., Gerardy-Schahn, R. and von Itzstein, M. (2007) Direct detection of ligand binding to Sepharose-immobilised protein using saturation transfer double difference (STDD) NMR spectroscopy. *Biochem. Biophys. Res. Commun.* **359**, 866–870 [CrossRef](#) [PubMed](#)
- 66 Pereira, A., Pfeifer, T.A., Grigliatti, T.A. and Andersen, R.J. (2009) Functional cell-based screening and saturation transfer double-difference NMR have identified haplosamate A as a cannabinoid receptor agonist. *ACS Chem. Biol.* **4**, 139–144 [CrossRef](#) [PubMed](#)
- 67 Shirzadi, A., Simpson, M.J., Xu, Y. and Simpson, A.J. (2008) Application of saturation transfer double difference NMR to elucidate the mechanistic interactions of pesticides with humic acid. *Environ. Sci. Technol.* **42**, 1084–1090 [CrossRef](#) [PubMed](#)
- 68 Venkitakrishnan, R., Benard, O., Max, M., Markley, J. and Assadi-Porter, F. (2012) Use of NMR saturation transfer difference spectroscopy to study ligand binding to membrane proteins. *Membrane Protein Structure and Dynamics* (Vaidehi, N. and Klein-Seetharaman, J., eds), pp. 47–63, Humana Press, Totowa, NJ [CrossRef](#)
- 69 Ritchie, T.K., Grinkova, Y.V., Bayburt, T.H., Denisov, I.G., Zolnerciks, J.K., Atkins, W.M. and Sliagar, S.G. (2009) Reconstitution of membrane proteins in phospholipid bilayer nanodiscs. *Methods Enzymol.* **464**, 211–231 [CrossRef](#) [PubMed](#)
- 70 Borgnia, M.J., Eytan, G.D. and Assaraf, Y.G. (1996) Competition of hydrophobic peptides, cytotoxic drugs, and chemosensitizers on a common P-glycoprotein pharmacophore as revealed by its ATPase activity. *J. Biol. Chem.* **271**, 3163–3171 [CrossRef](#) [PubMed](#)
- 71 Litman, T., Zeuthen, T., Skovsgaard, T. and Stein, W.D. (1997) Structure–activity relationships of P-glycoprotein interacting drugs: kinetic characterization of their effects on ATPase activity. *Biochim. Biophys. Acta* **1361**, 159–168 [CrossRef](#) [PubMed](#)
- 72 Orłowski, S., Mir, L.M., Belehradek, Jr, J. and Garrigos, M. (1996) Effects of steroids and verapamil on P-glycoprotein ATPase activity: progesterone, desoxycorticosterone, corticosterone and verapamil are mutually non-exclusive modulators. *Biochem. J.* **317** (Pt 2), 515–522 [CrossRef](#) [PubMed](#)
- 73 Sharom, F.J., Yu, X., Chu, J.W. and Doige, C.A. (1995) Characterization of the ATPase activity of P-glycoprotein from multidrug-resistant Chinese hamster ovary cells. *Biochem. J.* **308** (Pt 2), 381–390 [CrossRef](#) [PubMed](#)
- 74 Litman, T., Nielsen, D., Skovsgaard, T., Zeuthen, T. and Stein, W.D. (1997) ATPase activity of P-glycoprotein related to emergence of drug resistance in Ehrlich ascites tumor cell lines. *Biochim. Biophys. Acta* **1361**, 147–158 [CrossRef](#) [PubMed](#)
- 75 Romsicki, Y. and Sharom, F.J. (1999) The membrane lipid environment modulates drug interactions with the P-glycoprotein multidrug transporter. *Biochemistry* **38**, 6887–6896 [CrossRef](#) [PubMed](#)
- 76 Doige, C.A., Yu, X. and Sharom, F.J. (1993) The effects of lipids and detergents on ATPase-active P-glycoprotein. *Biochim. Biophys. Acta* **1146**, 65–72 [CrossRef](#) [PubMed](#)
- 77 Saeki, T., Shimabuku, A.M., Ueda, K. and Komano, T. (1992) Specific drug binding by purified lipid-reconstituted P-glycoprotein: dependence on the lipid composition. *Biochim. Biophys. Acta* **1107**, 105–110 [CrossRef](#) [PubMed](#)
- 78 Romsicki, Y. and Sharom, F.J. (1998) The ATPase and ATP-binding functions of P-glycoprotein—modulation by interaction with defined phospholipids. *Eur. J. Biochem.* **256**, 170–178 [CrossRef](#) [PubMed](#)
- 79 Sharom, F.J. (2014) Complex interplay between the P-glycoprotein multidrug efflux pump and the membrane: its role in modulating protein function. *Front. Oncol.* **4**, 41 [CrossRef](#) [PubMed](#)



- 80 Matsunaga, T., Kose, E., Yasuda, S., Ise, H., Ikeda, U. and Ohmori, S. (2006) Determination of P-glycoprotein ATPase activity using Luciferase. *Biol. Pharm. Bull.* **29**, 560–564 [CrossRef PubMed](#)
- 81 Rebbear, J.F. and Senior, A.E. (1998) Effects of cardiovascular drugs on ATPase activity of P-glycoprotein in plasma membranes and in purified reconstituted form. *Biochim. Biophys. Acta* **1369**, 85–93 [CrossRef PubMed](#)
- 82 von Richter, O., Glavinias, H., Krajcsi, P., Liehner, S., Siewert, B. and Zech, K. (2009) A novel screening strategy to identify ABCB1 substrates and inhibitors. *Naunyn Schmiedeberg's Arch. Pharmacol.* **379**, 11–26 [CrossRef PubMed](#)
- 83 Hansen, T.S. and Nilsen, O.G. (2009) Echinacea purpurea and P-glycoprotein drug transport in Caco-2 cells. *Phytother. Res.* **23**, 86–91 [CrossRef PubMed](#)
- 84 Loo, T.W., Bartlett, M.C. and Clarke, D.M. (2003) Simultaneous binding of two different drugs in the binding pocket of the human multidrug resistance P-glycoprotein. *J. Biol. Chem.* **278**, 39706–39710 [CrossRef PubMed](#)
- 85 Loo, T.W., Bartlett, M.C. and Clarke, D.M. (2003) Substrate-induced conformational changes in the transmembrane segments of human P-glycoprotein. Direct evidence for the substrate-induced fit mechanism for drug binding. *J. Biol. Chem.* **278**, 13603–13606 [CrossRef PubMed](#)
- 86 Loo, T.W., Bartlett, M.C. and Clarke, D.M. (2003) Drug binding in human P-glycoprotein causes conformational changes in both nucleotide-binding domains. *J. Biol. Chem.* **278**, 1575–1578 [CrossRef PubMed](#)
- 87 Wang, G., Pincheira, R. and Zhang, J.T. (1998) Dissection of drug-binding-induced conformational changes in P-glycoprotein. *Eur. J. Biochem.* **255**, 383–390 [CrossRef PubMed](#)
- 88 Nagy, H., Goda, K., Arcesi, R., Cianfriglia, M., Mechetner, E. and Szabo, Jr. G. (2001) P-Glycoprotein conformational changes detected by antibody competition. *Eur. J. Biochem.* **268**, 2416–2420 [CrossRef PubMed](#)
- 89 Verhalen, B., Ernst, S., Borsch, M. and Wilkens, S. (2012) Dynamic ligand-induced conformational rearrangements in P-glycoprotein as probed by fluorescence resonance energy transfer spectroscopy. *J. Biol. Chem.* **287**, 1112–1127 [CrossRef PubMed](#)
- 90 Ritchie, T.K., Kwon, H. and Atkins, W.M. (2011) Conformational analysis of human ATP-binding cassette transporter ABCB1 in lipid nanodiscs and inhibition by the antibodies MRK16 and UIC2. *J. Biol. Chem.* **286**, 39489–39496 [CrossRef PubMed](#)
- 91 Loo, T.W., Bartlett, M.C. and Clarke, D.M. (2002) The “LSGGQ” motif in each nucleotide-binding domain of human P-glycoprotein is adjacent to the opposing Walker A sequence. *J. Biol. Chem.* **277**, 41303–41306 [CrossRef PubMed](#)
- 92 Loo, T.W., Bartlett, M.C., Detty, M.R. and Clarke, D.M. (2012) The ATPase activity of the P-glycoprotein drug pump is highly activated when the N-terminal and central regions of the nucleotide-binding domains are linked closely together. *J. Biol. Chem.* **287**, 26806–26816 [CrossRef PubMed](#)
- 93 Urbatsch, I.L., Sankaran, B., Bhagat, S. and Senior, A.E. (1995) Both P-glycoprotein nucleotide-binding sites are catalytically active. *J. Biol. Chem.* **270**, 26956–26961 [CrossRef PubMed](#)
- 94 Hrycyna, C.A., Ramachandra, M., Germann, U.A., Cheng, P.W., Pastan, I. and Gottesman, M.M. (1999) Both ATP sites of human P-glycoprotein are essential but not symmetric. *Biochemistry* **38**, 13887–13899 [CrossRef PubMed](#)
- 95 Lawson, J., O'Mara, M.L. and Kerr, I.D. (2008) Structure-based interpretation of the mutagenesis database for the nucleotide binding domains of P-glycoprotein. *Biochim. Biophys. Acta* **1778**, 376–391 [CrossRef PubMed](#)
- 96 Beaudet, L. and Gros, P. (1995) Functional dissection of P-glycoprotein nucleotide-binding domains in chimeric and mutant proteins. Modulation of drug resistance profiles. *J. Biol. Chem.* **270**, 17159–17170 [CrossRef PubMed](#)
- 97 Welker, E., Szabo, K., Hollo, Z., Muller, M., Sarkadi, B. and Varadi, A. (1995) Drug-stimulated ATPase activity of a deletion mutant of the human multidrug-resistance protein (MDR1). *Biochem. Biophys. Res. Commun.* **216**, 602–609 [CrossRef PubMed](#)
- 98 Loo, T.W., Bartlett, M.C. and Clarke, D.M. (2003) Permanent activation of the human P-glycoprotein by covalent modification of a residue in the drug-binding site. *J. Biol. Chem.* **278**, 20449–20452 [CrossRef PubMed](#)
- 99 Hafkemeyer, P., Dey, S., Ambudkar, S.V., Hrycyna, C.A., Pastan, I. and Gottesman, M.M. (1998) Contribution to substrate specificity and transport of nonconserved residues in transmembrane domain 12 of human P-glycoprotein. *Biochemistry* **37**, 16400–16409 [CrossRef PubMed](#)
- 100 Omote, H., Figler, R.A., Polar, M.K. and Al-Shawi, M.K. (2004) Improved energy coupling of human P-glycoprotein by the glycine 185 to valine mutation. *Biochemistry* **43**, 3917–3928 [CrossRef PubMed](#)
- 101 Rao, U.S. (1995) Mutation of glycine 185 to valine alters the ATPase function of the human P-glycoprotein expressed in Sf9 cells. *J. Biol. Chem.* **270**, 6686–6690 [PubMed](#)
- 102 Wang, Q., Rager, J.D., Weinstein, K., Kardos, P.S., Dobson, G.L., Li, J. and Hidalgo, I.J. (2005) Evaluation of the MDR-MDCK cell line as a permeability screen for the blood-brain barrier. *Int. J. Pharm.* **288**, 349–359 [CrossRef PubMed](#)
- 103 Taub, M.E., Podila, L., Ely, D. and Almeida, I. (2005) Functional assessment of multiple P-glycoprotein (P-gp) probe substrates: influence of cell line and modulator concentration on P-gp activity. *Drug Metab. Dispos.* **33**, 1679–1687 [CrossRef PubMed](#)

---

Received 21 December 2015/21 December 2015; accepted 22 January 2016

Accepted Manuscript online 27 January 2016, doi 10.1042/BSR20150317

---